materials

MDPI

Communication

Mechanochemical Synthesis of Pt/Nb_2CT_x MXene Composites for Enhanced Electrocatalytic Hydrogen Evolution

Xiaoyuan Fan [1,†], Peng Du [1,2,†], Xiaoxuan Ma [1,†], Ruyue Wang [1,2], Jingteng Ma [1], Yonggang Wang [1], Dongyu Fan [1], Yuanzheng Long [2], Bohan Deng [2], Kai Huang [1,*] and Hui Wu [2,*]

[1] State Key Laboratory of Information Photonics and Optical Communications, School of Science, Beijing University of Posts and Telecommunications, Beijing 100876, China; fxy2018212527@bupt.edu.cn (X.F.); pengdu@bupt.edu.cn (P.D.); kristenmxx@bupt.edu.cn (X.M.); Wang_Ruyue@bupt.edu.cn (R.W.); mjt2021@bupt.edu.cn (J.M.); wangyg@bupt.edu.cn (Y.W.); vandy@bupt.edu.cn (D.F.)

[2] State Key Laboratory of New Ceramics and Fine Processing, School of Materials, Science and Engineering, Tsinghua University, Beijing 100084, China; longyz19@mails.tsinghua.edu.cn (Y.L.); dbh20@mails.tsinghua.edu.cn (B.D.)

* Correspondence: huang-kai@bupt.edu.cn (K.H.); huiwu@mail.tsinghua.edu.cn (H.W.)

† These authors contribute equally to this work.

Abstract: Production of hydrogen from water splitting has been considered as a promising solution for energy conversion and storage. Since a noble metal-based structure is still the most satisfactory but scarce kind of catalyst, it is significant to allow for practical application of such catalysts by engineering the heterogeneous structure and developing green and facile synthetic strategies. Herein, we report a mechanochemical ball milling synthesis of platinum nanoclusters immobilized on a 2D transition metal carbide MXene (Nb_2CT_x) as an enhanced catalyst for hydrogen evolution. After annealing at 600 °C, ultrafine Pt_3Nb nanoclusters are formed on the Pt/Nb_2CT_x catalyst. As prepared, the Pt/Nb_2CT_x-600 catalyst demonstrates superior electrochemical HER activity and stability with an ultralow overpotential of 5 mV and 46 mV to achieve 10 mA cm^{-2} and 100 mA cm^{-2}, respectively, in comparison with other Nb_2CT_x-based catalysts and commercial Pt/C catalysts. Moreover, the remarkable durability is also confirmed by accelerated durability tests (ADTs) and long-term chronoamperometry (CA) tests. The excellent HER performance was attributed to high Pt dispersion and more active site exposure by the mechanochemical process and thermal treatment. Such results suggest that the mechanochemical strategy provides a novel approach for rational design and cost-effective production of electrocatalysts, also providing other potential applications in a wide range of areas.

Keywords: hydrogen evolution; Pt-Nb alloy; mechanochemical synthesis; thermal annealing

Citation: Fan, X.; Du, P.; Ma, X.; Wang, R.; Ma, J.; Wang, Y.; Fan, D.; Long, Y.; Deng, B.; Huang, K.; et al. Mechanochemical Synthesis of Pt/Nb_2CT_x MXene Composites for Enhanced Electrocatalytic Hydrogen Evolution. *Materials* **2021**, *14*, 2426. https://doi.org/10.3390/ma14092426

Academic Editor: Enrico Negro

Received: 30 March 2021
Accepted: 28 April 2021
Published: 6 May 2021

1. Introduction

With the development of modern industry, a rapidly increasing demand for energy has become one of the most significant problems affecting the life of human beings [1,2]. Hydrogen has received substantial attention as a renewable and completely clean energy carrier, making it a favorable candidate for replacing traditional fossil fuels and a promising solution for alleviating environmental crisis [3–5]. The production of hydrogen from water splitting represents a highly efficient and sustainable approach to deal with this concern. Thus, novel hydrogen evolution reaction (HER) electro-catalysts exhibiting excellent activity and long durability, along with a green and scalable synthesis strategy, are highly desired for the realization of clean energy infrastructure and application [6,7].

In the past few years, state-of-the-art noble metal-free catalysts with high HER activity have been extensively reported, consisting of carbon-based nanostructures, metal phosphides, MoS_2, transition metal oxides and related compounds [8–12]. Nevertheless, noble metal platinum-based catalysts are still the most promising HER electrocatalysts currently,

due to their advantageous catalytic activity and selectivity, but the extremely high costs, difficulty of engineering and mass-producing desirable structures with high performance seriously obstruct industrial application [13]. As we know, electrocatalytic reaction occurs on the surface and interface of the catalyst, while in the process of preparation and long-term working noble metal nanoclusters or particles supported on substrate materials are prone to agglomeration, or active sites are blocked due to high surface free energy, which causes the active noble metal component to exist in the form of larger aggregates, leading to loss of catalytic activity [14–16]. In addition, the preparation of such supported noble metal catalysts generally requires complicated procedures, complicated experimental conditions (such as high annealing temperature and pressure) and the use of a large number of organic solvents or capping agents, making the processing inefficient in time and costs, and even bringing environmental problems [17,18]. Moreover, it is a challenge to apply synthetic routes from a laboratory scenario to large-scale industrial production, since the scale-up effect will make it difficult to delicately control the size and dispersity of noble metal nanostructures on supports [19]. The problems mentioned above have appreciably limited the large-scale application of such catalysts in practical scenarios. Therefore, it is urgent to design a geometric and electronic structure for supported noble metal catalysts and develop an economical and facile synthetic strategy for catalysts.

As types of newly emerging 2D material, MXenes, early transition-metal carbides (M) and carbonitrides (M) have a well-defined structure and a wide range of adjustable components and have received substantial attention. The general formula of MXene is $M_{n+1}X_nT_x$ (n = 2–4); the layers containing the transition metals are exposed outside of the structure and T_x generally stands for surface termination groups containing OH*, O* and F* [20,21]. The excellent electronic conductivity, volumetric capacitance, and chemical stability of MXene make it favorable as a promising support material for metal nanostructures and it is widely used in energy conversion and storage, sensing, biomedicine and other fields [22–24]. The mechanical exfoliation and downsizing of layered MXene at room temperature can significantly expose more electrochemical active sites and increase surface-to-volume ratio. At the same time, the noble metal nanostructures are compounded, which can optimize the dispersion of noble metal species and the formation of a metal-support interface with high thermal stability [25].

The existence of noble metal nanostructures (single atoms, clusters or nanoparticles) not only promotes the removal of surface functional groups but also accelerates the electron transfer between MXene support and Pt nanoclusters [26]. Furthermore, metal-support interactions (MSIs) can become enhanced through thermal annealing under inert conditions at a moderate temperature, meanwhile generating a Pt-M (early transition metal) alloy composition and preventing aggregation of the noble metal structure [27,28]. Therefore, MXene was adopted as substrate material and simultaneously achieved the exfoliation of 2D layers of a smaller size, as well as immobilization of noble metal nanostructures by a mechanochemical process, providing an optimized interface area and improvement of MSIs, which paves the way for superior HER performance.

In this study, we developed a mechanochemical ball milling synthesis to fabricate a Pt-based Nb_2CT_x MXene composite, the Pt loading amount of which was 1.0 wt%. Subsequently thermal treatment at 600 °C guarantees the rearrangement of atoms and electrons on the surface of the Pt and Nb_2CT_x substrate, forming a small-sized Pt_3Nb alloy with an average size of only 2.1 nm. Electrochemical tests showed that the catalyst possessed superior HER performance and long-term stability in acidic electrolyte. This work provides a simple and universal mechanochemical strategy for the large-scale preparation of transition metal-Pt alloy supported MXene composite catalyst with a wide range of compositions and structures, which also expands the practical application of such catalysts in diverse fields.

2. Materials and Methods

2.1. Materials

Nb_2CT_x (55–70 wt%, XFNANO, Nanjing, China), Chloroplatinic acid ($H_2PtCl_6 \cdot 6H_2O$, AR, Pt $\geq$ 37.5%, Aladdin, Shanghai, China), and absolute ethanol (C_2H_5OH, 99.8%, Aladdin, Shanghai, China) were used as received without any further purification.

2.2. Preparation of Nb_2CT_x Based Catalysts

Typically, for the ball milling synthesis of Pt/Nb_2CT_x, 500 mg of bulk Nb_2CT_x powder was immersed into 30 cm^3 of absolute ethanol and sonicated by a high-power ultrasonic probe for 30 min to form a homogenous suspension. Then 420 uL of 0.1 mol/L solution of chloroplatinic acid was introduced into as-prepared suspension and continuously stirred for 40 min. The mixed solution was then transferred into a corundum tank and ball-milled at a speed of 150 rpm for about 30 min. Finally, the Pt/Nb_2CT_x sample was obtained by vacuum filtration and then drying the solution. The as-prepared Pt/Nb_2CT_x catalyst was annealed at 600 °C for 2 h with a heating rate of 1 °C min^{-1} under flowing Ar gas to obtain the sample denoted as Pt/Nb_2CT_x-600.

2.3. Characterizations of Nb_2CT_x Based Catalysts

The morphology, microstructure and chemical composition of the as-prepared catalysts were characterized by energy dispersion spectroscopy (EDS) elemental mapping images taken by aberration-corrected high-resolution transmission electron microscopy (HRTEM, JEOL, Tokyo, Japan, JEM-ARM200F), as well as a field emission scanning electron microscope (FE-SEM, LEO-1530, Zeiss, Oberkochen, Germany). The structural characterization of catalysts was performed by powder X-ray diffractometry (XRD, RIGAKU, Tokyo, Japan, D/max 2500 V) using Cu Ka as radiation source, and X-ray photoelectron spectroscopy (XPS, ESCALAB 250Xi, Thermo Scientific, Waltham, MA, USA). Inductively coupled plasma atomic emission spectrometry (ICP-AES) analysis was performed on a Thermo ICAP-6300 instrument (Thermo Electron Limited, Cambridge, UK). The electrocatalytic measurements of Nb_2CT_x based catalysts are shown in the Supplementary Materials.

3. Results

The synthetic procedure for Pt/Nb_2CT_x including ball milling and thermal treatment is illustrated in Figure 1. We employed ethanol with slow reduction kinetics to guarantee that the H_2PtCl_6 precursor was chemically reduced into relatively small sized nanostructures and adequately combined with the Nb_2CT_x substrate [29]. The solution of H_2PtCl_6 and Nb_2CT_x was directly transferred into a corundum tank for further ball milling at room temperature. As shown in Figure S1, the SEM images of Pt/Nb_2CT_x after the ball milling processes indicate that the bulky layered Nb_2CT_x MXene materials can be partly exfoliated into an island structure with an average size of about 500 nm, which is closely correlated with the fully exposure of active sites. Moreover, the appropriate mechanical force in the process plays an important role in controlling the Pt nanocluster's size and distribution [30]. In the next step, as-prepared Pt/Nb_2CT_x was annealed in Ar atmosphere at 600 °C (designated as Pt/Nb_2CT_x-600) to obtain thermally stable Pt-Nb alloys and optimize the electrochemical HER performance. The morphology of Pt and Nb_2CT_x compounds was firstly investigated by transmission electron microscopy (TEM). The TEM images of Pt/Nb_2CT_x-600 catalyst at different magnifications are shown in Figure 2a–c, and metallic nanoclusters can be observed, well dispersed onto the surface of Nb_2CT_x substrate, the average diameter of which is about 1.5 nm. As shown in Figure S2, we also observed metallic nanoclusters of similar size immobilized on the surface of substrate materials for the Pt/Nb_2CT_x catalyst, indicating that Pt species might react with ethanol and anchor onto Nb_2CT_x during the mechanochemical ball milling procedure. Moreover, the homogeneous distribution of Pt nanoclusters was also revealed by the energy dispersive spectroscopy (EDS) elemental mapping of Nb, C and Pt elements in Figure 2d–f. The loading amount of Pt in the catalyst is as low as 1.0 wt%, which is determined by ICP-AES. As shown in

Figure 2g–i, high-resolution transmission electron microscopy (HRTEM) further proves that the existence of Pt_3Nb alloy nanoclusters successfully anchored on Nb_2CT_x with a typical size of about 1.2 nm and a representative crystal lattice indexed to (200) planes (0.22 nm in space) of Pt_3Nb alloy, which matches the schematic illustration and material design [31].

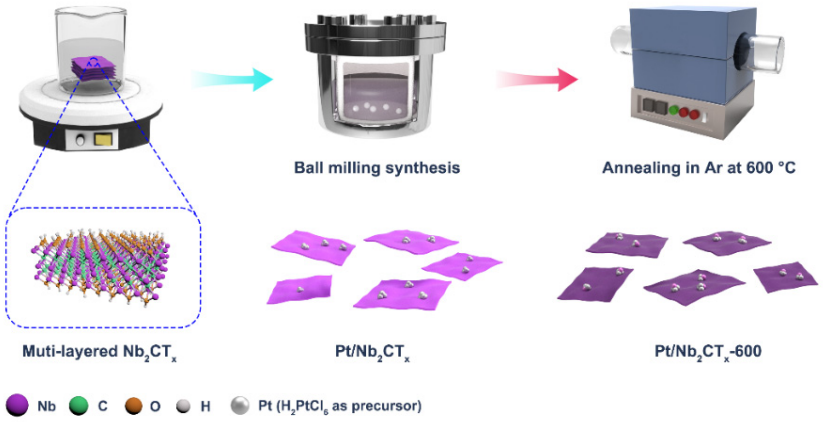

Figure 1. Schematic illustration of the preparation ofNb_2CT_x-600 catalyst by ball milling and thermal treatment.

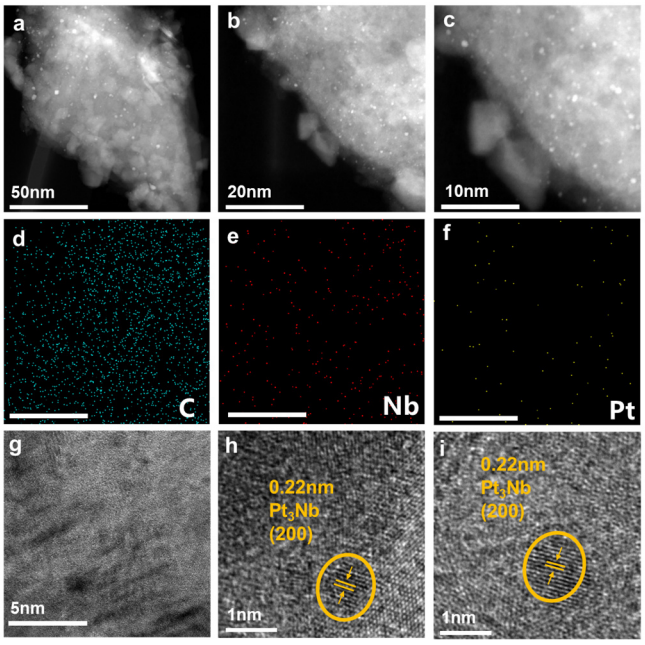

Figure 2. (**a**–**c**) TEM images of Pt/Nb_2CT_x-600; (**d**–**f**) EDS mapping images of Pt/Nb_2CT_x-600 (scale bar: 50 nm); (**g**–**i**) HRTEM of Pt/Nb_2CT_x-600.

As shown in Figure S3, selective area electron diffraction (SAED) was carried out to obtain more accurate information on the lattice, where both pristine Nb_2CT_x and Pt/Nb_2CT_x-600 samples show good crystallinity of the Nb_2CT_x ultrathin nanostructures. In addition, Figure S4 displays the intensity profile across the lattice of pristine Nb_2CT_x and Pt/ Nb_2CT_x, the similar grayscale value suggesting that the crystalline structure of the Pt/Nb_2CT_x-600 has not changed, while the appearance of peak at 2520 and 3112 μm^{-1} can be attributed to the formation of Pt_3Nb and the enhanced metal-support interaction.

X-ray diffraction (XRD) and X-ray photoelectron spectroscopy (XPS) characterizations were further investigated to obtain insight into the chemical state and coordination environment of as-prepared catalysts. As featured in Figure 3a, due to the abundant surface

termination groups T_x, the diffraction peaks of Nb_2CT_x were only partly consistent with the standard card of Nb_2C (shown in Figure S5). No obvious Pt phase could be identified in the XRD pattern of Pt/Nb_2CT_x, suggesting the homogeneous distribution of small-sized Pt nanoclusters, and no obvious changes were induced to the crystalline structure of Nb_2CT_x by the Pt modification. In comparison, the annealed Pt/Nb_2CT_x-600 sample exhibits a dramatic appearance of characteristic peaks corresponding to the standard card (JCPDS, PDF#78-0499) for Pt_3Nb alloy, the relatively weak signal of which can be attributed to the low Pt modification content [32]. This result confirms that Pt_3Nb alloy was generated due to annealing treatment in Ar at 600 °C, consistent with the HRTEM and SAED results. Figure S6 exhibits the whole spectrum survey of Pt/Nb_2CT_x and Pt/Nb_2CT_x-600 calibrated with the main peak of C 1s at 284.8 eV, indicating the existence of Nb, C, O, and F elements. In Figure 3b, the high-resolution Pt 4f XPS spectrum of Pt/Nb_2CT_x and the annealed catalyst are resolved into four peaks corresponding to Pt^0 in a metallic state existing on the surface of Nb_2CT_x along with some Pt^{2+} (Pt-O) species [33,34]. Compared with the Pt $4f_{7/2}$ spectrum of Pt/Nb_2CT_x catalyst, a shift toward higher binding energy (0.2~0.4 eV for Pt^0 and 0.1 eV for Pt^{2+}) can be notably observed for the annealed sample. The dominant existence of oxidation states of niobium can be brought out according to the Nb 3d spectrum in Figure 3c, which is due to the oxophilicity of Nb. For the unannealed catalyst, the Nb 3d XPS peak can be divided into two group components corresponding to Nb^{2+} (204.1, 207 eV) and Nb^{5+} (207.2, 210 eV), respectively. A positive shift (204.6/207.2 eV for Nb^{2+} and 207.6/210.2 eV for Nb^{5+}) can be detected after thermal treatment [35]. The above analysis of Pt 4f and Nb 3d XPS spectrum provides cogent evidence for the amplified metal-support interaction and formation of Pt-Nb alloy. In addition, the C 1s spectrum of Pt/Nb_2CT_x in Figure 3d is deconvoluted into four peaks attributing to C-Nb (281.6 eV), C-C (284.8 eV), C-O (286.2 eV) and C-F (288.8 eV). For the Pt/Nb_2CT_x-600, the near disappearance of the C-Nb typical peak can be markedly observed, suggesting the transfer of atoms and electrons between Nb_2CT_x substrate and Pt species under the thermal effect. The surface chemical states of C element also indicate the existence of surface termination groups before and after annealing [36].

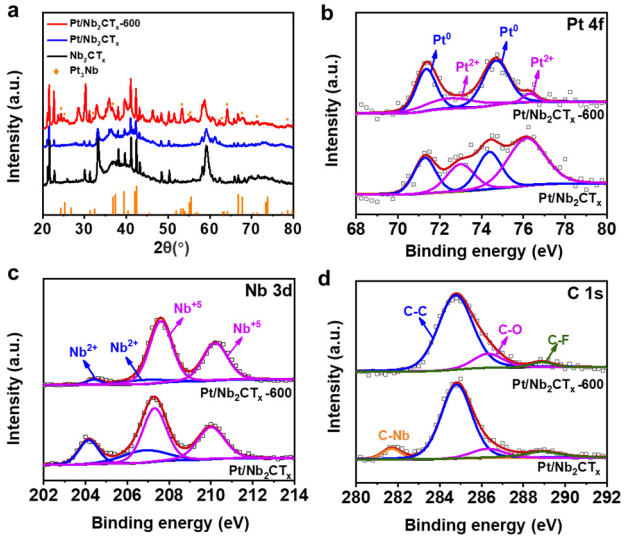

Figure 3. (**a**) XRD patterns of bulk Nb_2CT_x, Pt/Nb_2CT_x, Pt/Nb_2CT_x-600; (**b**–**d**) Pt 4f, Nb 3d, C 1s XPS spectrum of Pt/Nb_2CT_x and Pt/Nb_2CT_x-600 catalysts.

The electrocatalytic performance of the Pt/Nb_2CT_x-600 and related catalysts for hydrogen evolution reaction (HER) was evaluated using a three-electrode system in the 0.5 M H_2SO_4 electrolyte. Linear sweep voltammetry (LSV) is adopted to evaluate the HER activities of the catalysts as shown in Figure 4a. Significantly, the Pt/Nb_2CT_x-600 with homogeneous distributed Pt_3Nb alloys exhibits the superior HER activity compared

with Pt/Nb_2CT_x, Nb_2CT_x substrate and commercial Pt/C catalysts, requiring an overpotential of only 5 mV and 46 mV to reach a current density of 10 and 100 mA cm^{-2} (E_{j10} and E_{j100}), respectively, significantly better than the values for Pt/Nb_2CT_x (E_{j10} = 31 mV, E_{j100} = 115 mV) and commercial Pt/C catalyst (E_{j10} = 6.2 mV, E_{j100} = 82.4 mV). The results can further be demonstrated by Tafel plots derived from HER polarization curves in Figure 4b. A smaller Tafel slope of 34.66 mV dec^{-1} for Pt/Nb_2CT_x-600 than values of 45.07 mV dec^{-1} for Pt/C catalyst and 64.70 mV dec^{-1} for Pt/Nb_2CT_x has been verified following the Volmer-Tafel mechanism, indicating the rapid HER kinetics derived from the advantage of Pt_3Nb alloy phase. The reaction kinetic rate of catalysts was also evaluated by the electrochemical impedance spectroscopy (EIS) analysis in Figure 4c and Table S1, which is fitted using an equivalent circuit diagram consisting of the solution resistance (R_s), high-frequency interfacial charge transfer resistance (R_{ct1}) and low-frequency (R_2) element connected with H_2 mass-transport. The smaller R_{ct1} value for the Pt/Nb_2CT_x-600 than for the unannealed Pt/Nb_2CT_x delivers an excellent charge-transfer process between Pt-Nb interfaces [37]. In addition, the HER polarization curve and Tafel plot of the pristine Nb_2CT_x substrate are also revealed in Figures S7 and S8, respectively. When the overpotential was up to 500 mV, the pristine Nb_2CT_x catalyst achieved a current density of 36.3 mA cm^{-2} and the corresponding Tafel slope is 239.24 mV dec^{-1}, the performance of which is dramatically poorer than Pt immobilized catalysts, indicating that the immobilization of Pt species on the surface of Nb_2CT_x substrate by ball milling synthesis and further thermal treatment can effectively accelerate the charge transfer and kinetics of the catalytic process. Moreover, the excellent catalytic stability of Pt/Nb_2CT_x-600 was further convinced using typical accelerated durability tests (ADTs) and long-term chronoamperometry (CA) tests. The obtained polarization curves before and after 1000 and 5000 cycles are shown in Figure 4d, and there is no obvious decay in E_{j10} and E_{j100} after 5000 continuous potential cycles. The Pt/Nb_2CT_x-600 sample also displays small degradation of about 5% after 20 h CA test operations, compared with ~30% degradation for commercial Pt/C catalysts. As shown in Figures S9–S11, the structural stability of Pt/Nb_2CT_x-600 under HER conditions has been confirmed by HRTEM images, XPS and XRD characterizations after a 5k ADT cycles long-term stability test, demonstrating that the active site will not change during the reaction. Above all, the result of the electrochemical test revealed the prominent performance of the Pt/Nb_2CT_x-600 catalyst, attributed to the strong MSI between Pt and Nb_2CT_x and the formation of a Pt_3Nb alloy phase with high intrinsic activity [38]. As discussed above, all electro-catalysis results suggested the advanced HER performance of Pt/Nb_2CT_x-600 catalyst via ball milling and thermal treatment. With metal-support interaction, the formation of Pt-Nb alloy could improve the onset potential and benefit the formation of the active site, and the synergetic effect plays its own role in strongly adsorbing H* intermediate species and improves the intrinsic catalytic activity by accelerating kinetics, which will become the key for the synergistically promoted HER. Comparison of E_{j10}, E_{j100} and Tafel slope with other similar systems is listed in Table S2, confirming that the as-prepared Pt/Nb_2CT_x-600 outperformed the majority of other recently reported catalysts.

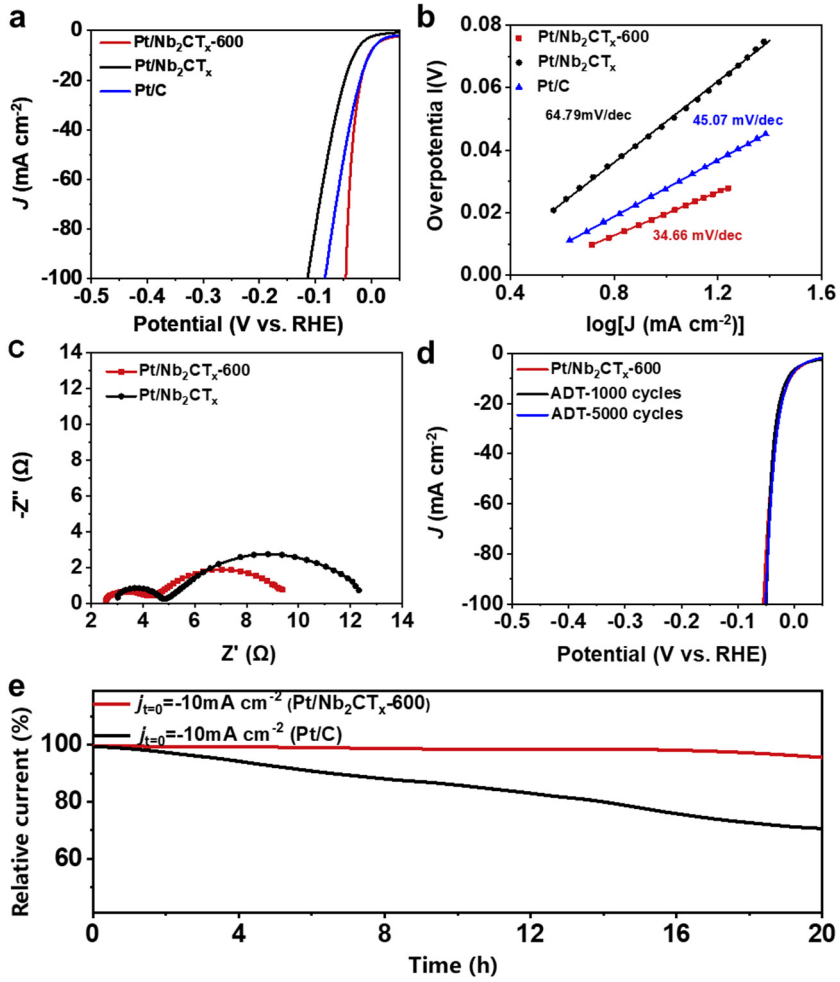

Figure 4. Electrocatalytic HER performance of different catalysts in 0.5 M H_2SO_4. (**a**) Polarization curves of the Pt/Nb_2CT_x, Pt/Nb_2CT_X-600, commercial Pt/C catalysts. (**b**) Tafel plots of the Pt/Nb_2CT_x, Pt/Nb_2CT_X-600, commercial Pt/C catalysts. (**c**) EIS Nyquist plots for HER performance of the Pt/Nb_2CT_x and Pt/Nb_2CT_X-600 catalysts. (**d**) ADT tests for HER performance of Pt/Nb_2CT_X-600 catalyst. (**e**) CA curves of Pt/Nb_2CT_x and Pt/C catalysts for HER performance.

4. Conclusions

In summary, we reported a simple mechanochemical ball milling and annealing strategy for the large-scale synthesis of Pt_3Nb alloy nanoclusters immobilized on the Nb_2CT_x substrate. The mechanical force and slow chemical kinetics during the process were conductive to the reduction and homogeneous dispersion of Pt species, as well as favoring the mass production of such supported noble metal catalysts. The subsequent thermal treatment in Ar enhanced the metal–support interaction between Pt nanoclusters and Nb_2CT_x substrates, forming Pt_3Nb alloy, the formation of which was verified by systematic morphology and structural characterization. The electrochemical experiment revealed that the prepared Pt/Nb_2CT_x catalyst exhibits the best HER activity with the lowest overpotential of 5 and 46 mV at the current density of 10 and 100 mA cm^{-2}, respectively, better than that of other Nb_2CT_x based catalysts and commercial Pt/C. Long-term stability is also demonstrated over 20 h CA tests and 5000 cycles of ADT tests. The superior performance can be ascribed to the enhanced metal–support interaction as well as the uniformly distributed Pt_3Nb alloy phase with small size and high intrinsic HER activity. The results suggest that the mechanochemical strategy provides a new approach for green and effective production of supported noble metal catalysts for energy conversion and storage applications.

Supplementary Materials: The following are available online at https://www.mdpi.com/article/10.3390/ma14092426/s1, Figure S1: Scanning electron microscopic (SEM) images of (a, b) bulk Nb_2CT_x; (c, d) Pt/ Nb_2CT_x catalyst synthesized by ball milling, Figure S2: Transmission electron microscopic (TEM) images of Pt/ Nb_2CT_x catalyst synthesized by ball milling, Figure S3: Selective area electron diffraction (SAED) of (**a**) pristine Nb_2CT_x and (**b**) Pt/ Nb_2CT_x-600, Figure S4: The intensity profile across the lattice of pristine Nb_2CT_x and Pt/ Nb_2CT_x, Figure S5: The XRD pattern of pristine Nb_2CT_x, Figure S6: The whole spectrum survey of Pt/Nb_2CT_x and Pt/Nb_2CT_x-600 calibrated with the main peak of C 1s at 284.8 eV, Figure S7: The HER polarization curve of the pristine Nb_2CT_x substrate, Figure S8: The HER Tafel plot of the pristine Nb_2CT_x substrate, Figure S9: TEM images of Pt/ Nb_2CT_x-600 after a 5k ADT cycles long-term stability test, Figure S10: XRD patterns of Pt/ Nb_2CT_x-600 and Pt/ Nb_2CT_x-600 after a 5k ADT cycles long-term stability test, Figure S11: Pt 4f XPS spectrum of Pt/ Nb_2CT_x-600 after a 5k ADT cycles long-term stability test, Table S1: The EIS fitting results of Pt/Nb_2CT_x and Pt/Nb_2CT_x-600 catalysts, Table S2: HER activity for recently reported noble metal catalysts in 0.5 M H_2SO_4 (* represents 0.1M H_2SO_4). References [39–57] are cited in the supplementary materials

Author Contributions: K.H., X.F., X.M. conceived and designed the experiments; X.F., J.M. and P.D. performed the experiments; P.D. and R.W. analyzed the data; Y.W., D.F., H.W., Y.L. and B.D. contributed reagents/materials/analysis tools; P.D. wrote the paper. All authors have read and agreed to the published version of the manuscript.

Funding: This research was funded by National Natural Science Foundations of China (Grant Nos. 61874013, 61974011 and 51902027), Fund of State Key Laboratory of Information Photonics and Optical Communications (Beijing University of Posts and Telecommunications. PR China), Basic Science Center Program of the National Natural Science Foundation of China (NSFC) (Grant No. 51788104), Beijing Natural Science Foundation (Grant No. JQ19005) and Science and Technology Plan of Shenzhen City (Grant No. JCYJ20180305164708625).

Institutional Review Board Statement: Not applicable.

Informed Consent Statement: Not applicable.

Data Availability Statement: The data presented in this study are available on request from the corresponding author.

Conflicts of Interest: The authors declare no conflict of interest. The funders had no role in the design of the study; in the collection, analyses, or interpretation of data; in the writing of the manuscript, or in the decision to publish the results.

References

1. Hosseini, S.E.; Wahid, M.A. Hydrogen production from renewable and sustainable energy resources: Promising green energy carrier for clean development. *Renew. Sustain. Energy Rev.* **2016**, *57*, 850–866. [CrossRef]
2. Chu, S.; Majumdar, A. Opportunities and challenges for a sustainable energy future. *Nature* **2012**, *488*, 294–303. [CrossRef] [PubMed]
3. Ahmad, H.; Kamarudin, S.K.; Minggu, L.J.; Kassim, M. Hydrogen from photo-catalytic water splitting process: A review. *Renew. Sustain. Energy Rev.* **2015**, *43*, 599–610. [CrossRef]
4. Turner, J.A. Sustainable hydrogen production. *Science* **2004**, *305*, 972–974. [CrossRef] [PubMed]
5. He, T.; Pachfule, P.; Wu, H.; Xu, Q.; Chen, P. Hydrogen carriers. *Nat. Rev. Mater.* **2016**, *1*, 16059. [CrossRef]
6. Yang, C.; Rousse, G.; Svane, K.L.; Pearce, P.E.; Abakumov, A.M.; Deschamps, M.; Cibin, G.; Chadwick, A.V.; Corte, D.A.D.; Hansen, H.A.; et al. Cation insertion to break the activity/stability relationship for highly active oxygen evolution reaction catalyst. *Nat. Commun.* **2020**, *11*, 1378. [CrossRef]
7. Jiao, Y.; Zheng, Y.; Jaroniec, M.; Qiao, S.Z. Design of electrocatalysts for oxygen-and hydrogen-involving energy conversion reactions. *Chem. Soc. Rev.* **2015**, *44*, 2060–2086. [CrossRef]
8. Huang, K.; Wang, R.; Zhao, S.; Du, P.; Wang, H.; Wei, H.; Long, Y.; Deng, B.; Lei, M.; Ge, B.; et al. Atomic species derived CoO_x clusters on nitrogen doped mesoporous carbon as advanced bifunctional electro-catalysts for Zn-air battery. *Energy Storage Mater.* **2020**, *29*, 156–162. [CrossRef]
9. Sun, Y.; Alimohammadi, F.; Zhang, D.; Guo, G. Enabling colloidal synthesis of edge-oriented MoS_2 with expanded interlayer spacing for enhanced HER catalysis. *Nano Lett.* **2017**, *17*, 1963–1969. [CrossRef]
10. Huang, K.; Xu, Y.; Song, Y.; Wang, R.; Wei, H.; Long, Y.; Lei, M.; Tang, H.; Guo, J.; Wu, H. $NiPS_3$ quantum sheets modified nitrogen-doped mesoporous carbon with boosted bifunctional oxygen electrocatalytic performance. *J. Mater. Sci. Technol.* **2021**, *65*, 1–6. [CrossRef]

11. Wang, X.; He, P.; Yang, Y.; Pan, Y.; Jin, Z.; Ling, R. Heterostructure Co_3O_4@ $NiWO_4$ nanocone arrays with enriched active area for efficient hydrogen evolution reaction. *J. Alloys Compd.* **2020**, *844*, 156095. [CrossRef]
12. Huang, K.; Guo, S.; Wang, R.; Lin, S.; Hussain, N.; Wei, H.; Deng, B.; Long, Y.; Lei, M.; Tang, H.; et al. Two-dimensional MOF/MOF derivative arrays on nickel foam as efficient bifunctional coupled oxygen electrodes. *Chin. J. Catal.* **2020**, *41*, 1754–1760. [CrossRef]
13. Li, M.; Duanmu, K.; Wan, C.; Cheng, T.; Zhang, L.; Dai, S.; Chen, W.; Zhao, Z.; Li, P.; Fei, H.; et al. Single-atom tailoring of platinum nanocatalysts for high-performance multifunctional electrocatalysis. *Nat. Catal.* **2019**, *2*, 495–503. [CrossRef]
14. Duan, H.; Li, D.; Tang, Y.; He, Y.; Ji, S.; Wang, R.; Lv, H.; Lopes, P.P.; Paulikas, A.P.; Li, H.; et al. High-performance Rh2P electrocatalyst for efficient water splitting. *J. Am. Chem. Soc.* **2017**, *139*, 5494–5502. [CrossRef] [PubMed]
15. Wu, Y.; Wang, D.; Li, Y. Understanding of the major reactions in solution synthesis of functional nanomaterials. *Sci. China Mater.* **2016**, *59*, 938–996. [CrossRef]
16. Campbell, C.T.; Parker, S.C.; Starr, D.E. The effect of size-dependent nanoparticle energetics on catalyst sintering. *Science* **2002**, *298*, 811–814. [CrossRef] [PubMed]
17. Wang, Q.; Ming, M.; Niu, S.; Zhang, Y.; Fan, G.; Hu, J.S. Scalable Solid-State Synthesis of Highly Dispersed Uncapped Metal (Rh, Ru, Ir) Nanoparticles for Efficient Hydrogen Evolution. *Adv. Energy Mater.* **2018**, *8*, 1801698. [CrossRef]
18. García-Peña, N.G.; Redón, R.; Herrera-Gomez, A.; Fernández-Osorio, A.L.; Bravo-Sanchez, M.; Gomez-Sosa, G. Solventless synthesis of ruthenium nanoparticles. *Appl. Surf. Sci.* **2015**, *340*, 25–34. [CrossRef]
19. Shi, D.; Yang, M.; Chang, B.; Ai, Z.; Zhang, K.; Shao, Y.; Wang, S.; Wu, Y.; Hao, X. Ultrasonic-Ball Milling: A Novel Strategy to Prepare Large-Size Ultrathin 2D Materials. *Small* **2020**, *16*, 1906734. [CrossRef] [PubMed]
20. Gao, G.; O'Mullane, A.P.; Du, A. 2D MXenes: A new family of promising catalysts for the hydrogen evolution reaction. *ACS Catal.* **2017**, *7*, 494–500. [CrossRef]
21. Seh, Z.W.; Fredrickson, K.D.; Anasori, B.; Kibsgaard, J.; Strickler, A.L.; Lukatskaya, M.R.; Gogotsi, Y.; Jaramillo, T.F.; Vojvodic, A. Two-dimensional molybdenum carbide (MXene) as an efficient electrocatalyst for hydrogen evolution. *ACS Energy Lett.* **2016**, *1*, 589–594. [CrossRef]
22. Xiu, L.; Pei, W.; Zhou, S.; Wang, Z.; Yang, P.; Zhao, J.; Qiu, J. Multilevel Hollow MXene Tailored Low-Pt Catalyst for Efficient Hydrogen Evolution in Full-pH Range and Seawater. *Adv. Funct. Mater.* **2020**, *30*, 1910028. [CrossRef]
23. Yin, J.; Pan, S.; Guo, X.; Gao, Y.; Zhu, D.; Yang, Q.; Gao, J.; Zhang, C.; Chen, Y. Nb_2C MXene-Functionalized Scaffolds Enables Osteosarcoma Phototherapy and Angiogenesis/Osteogenesis of Bone Defects. *Nano-Micro Lett.* **2021**, *13*, 30. [CrossRef]
24. Vaghasiya, J.V.; Mayorga-Martinez, C.C.; Vyskočil, J.; Sofer, Z.; Pumera, M. Integrated Biomonitoring Sensing with Wearable Asymmetric Supercapacitors Based on Ti_3C_2 MXene and 1T-Phase WS_2 Nanosheets. *Adv. Funct. Mater.* **2020**, *30*, 2003673. [CrossRef]
25. Zeng, Z.; Wang, C.; Siqueira, G.; Han, D.; Huch, A.; Abdolhosseinzadeh, S.; Heier, J.; Nüesch, F.; Zhang, C.; Nyström, G. Nanocellulose-MXene Biomimetic Aerogels with Orientation-Tunable Electromagnetic Interference Shielding Performance. *Adv. Sci.* **2020**, *7*, 2000979. [CrossRef] [PubMed]
26. Penner, S.; Armbrüster, M. Formation of intermetallic compounds by reactive metal–support interaction: A frequently encountered phenomenon in catalysis. *ChemCatChem* **2015**, *7*, 374–392. [CrossRef]
27. Li, Z.; Yu, L.; Milligan, C.; Ma, T.; Zhou, L.; Cui, Y.; Qi, Z.; Libretto, N.; Xu, B.; Luo, J.; et al. Two-dimensional transition metal carbides as supports for tuning the chemistry of catalytic nanoparticles. *Nat. Commun.* **2018**, *9*, 5258. [CrossRef]
28. Li, Z.; Cui, Y.; Wu, Z.; Milligan, C.; Zhou, L.; Mitchell, G.; Xu, B.; Shi, E.; Miller, J.T.; Ribeiro, F.H.; et al. Reactive metal–support interactions at moderate temperature in two-dimensional niobium-carbide-supported platinum catalysts. *Nat. Catal.* **2018**, *1*, 349–355. [CrossRef]
29. Chen, J.; Herricks, T.; Xia, Y. Polyol synthesis of platinum nanostructures: Control of morphology through the manipulation of reduction kinetics. *Angew. Chem. Int. Ed.* **2005**, *44*, 2589–2592. [CrossRef] [PubMed]
30. He, X.; Deng, Y.; Zhang, Y.; He, Q.; Xiao, D.; Peng, M.; Zhao, Y.; Zhang, H.; Luo, R.; Gan, T.; et al. Mechanochemical kilogram-scale synthesis of noble metal single-atom catalysts. *Cell Rep. Phys. Sci.* **2020**, *1*, 100004. [CrossRef]
31. Xu, S.L.; Shen, S.C.; Xiong, W.; Zhao, S.; Zuo, L.J.; Wang, L.; Zeng, W.J.; Chu, S.Q.; Chen, P.; Lin, Y.; et al. High-Temperature Synthesis of Small-Sized Pt/Nb Alloy Catalysts on Carbon Supports for Hydrothermal Reactions. *Inorg. Chem.* **2020**, *59*, 15953–15961. [CrossRef] [PubMed]
32. Ghoshal, S.; Jia, Q.; Bates, M.K.; Li, J.; Xu, C.; Gath, K.; Yang, J.; Waldecker, J.; Che, H.; Liang, W.; et al. Tuning Nb–Pt interactions to facilitate fuel cell electrocatalysis. *ACS Catal.* **2017**, *7*, 4936–4946. [CrossRef]
33. Cheng, X.; Li, Y.; Zheng, L.; Yan, Y.; Zhang, Y.; Chen, G.; Sun, S.; Zhang, J. Highly active, stable oxidized platinum clusters as electrocatalysts for the hydrogen evolution reaction. *Energy Environ. Sci.* **2017**, *10*, 2450–2458. [CrossRef]
34. Zhang, X.; Shao, B.; Sun, Z.; Gao, Z.; Qin, Y.; Zhang, C.; Cui, F.; Yang, X. Platinum Nanoparticle-Deposited $Ti_3C_2T_x$ MXene for Hydrogen Evolution Reaction. *Ind. Eng. Chem. Res.* **2020**, *59*, 1822–1828.
35. Wang, C.K.; Sahu, D.; Wang, S.C.; Huang, J.L. Electrochromic Nb-doped WO_3 films: Effects of post annealing. *Ceram. Int.* **2012**, *38*, 2829–2833.
36. Su, T.; Peng, R.; Hood, Z.D.; Naguib, M.; Ivanov, I.N.; Keum, J.K.; Qin, Z.; Guo, Z.; Wu, Z. One-step synthesis of $Nb_2O_5/C/Nb_2C$ (MXene) composites and their use as photocatalysts for hydrogen evolution. *ChemSusChem* **2018**, *11*, 688–699. [PubMed]

37. Huang, K.; Zhao, Z.; Du, H.; Du, P.; Wang, H.; Wang, R.; Lin, S.; Wei, H.; Long, Y.; Lei, M.; et al. Rapid thermal annealing toward high-quality 2D cobalt fluoride oxide as an advanced oxygen evolution electrocatalyst. *ACS Sustain. Chem. Eng.* **2020**, *8*, 6905–6913.
38. Kang, Y.J.; Jung, S.C.; Kim, H.J.; Han, Y.K.; Oh, S.H. Maximum catalytic activity of Pt_3M in Li-O_2 batteries: M=group V transition metals. *Nano Energy* **2016**, *27*, 1–7. [CrossRef]
39. Yu, F.Y.; Lang, Z.L.; Yin, L.Y.; Feng, K.; Xia, Y.J.; Tan, H.Q.; Zhu, H.T.; Zhong, J.; Kang, Z.H.; Li, Y.J. Pt-O bond as an active site superior to Pt^0 in hydrogen evolution reaction. *Nat. Commun.* **2020**, *11*, 490. [CrossRef] [PubMed]
40. Pu, Z.; Amiinu, I.S.; Kou, Z.; Li, W.; Mu, S. RuP_2-based catalysts with platinum-like activity and higher durability for the hydrogen evolution reaction at all pH values. *Angew. Chem. Int. Ed.* **2017**, *56*, 11559–11564.
41. Ji, J.; Zhang, Y.; Tang, L.; Liu, C.; Gao, X.; Sun, M.; Zhang, J.; Ling, M.; Liang, C.; Lin, Z. Platinum single-atom and cluster anchored on functionalized MWCNTs with ultrahigh mass efficiency for electrocatalytic hydrogen evolution. *Nano Energy* **2019**, *63*, 103849. [CrossRef]
42. Park, J.; Lee, S.; Kim, H.E.; Cho, A.; Kim, S.; Ye, Y.; Wan, J.W.; Lee, H.; Jiang, J.H.; Lee, J. Investigation of the support effect in atomically dispersed Pt on WO_{3-x} for utilization of Pt in the hydrogen evolution reaction. *Angew. Chem.* **2019**, *131*, 16184–16188. [CrossRef]
43. Xie, C.; Chen, W.; Du, S.; Yan, D.; Zhang, Y.; Chen, J.; Liu, B.; Wang, S. In-situ phase transition of WO_3 boosting electron and hydrogen transfer for enhancing hydrogen evolution on Pt. *Nano Energy* **2020**, *71*, 104653. [CrossRef]
44. Li, Z.; Qi, Z.; Wang, S.; Ma, T.; Zhou, L.; Wu, Z.; Luan, X.; Lin, F.Y.; Chen, M.; Miller, J.T. In situ formed Pt_3Ti nanoparticles on a two-dimensional transition metal carbide (MXene) used as efficient catalysts for hydrogen evolution reactions. *Nano Lett.* **2019**, *19*, 5102–5108. [CrossRef]
45. Han, J.; Meng, X.; Lu, L.; Wang, Z.L.; Sun, C. Triboelectric nanogenerators powered electrodepositing tri-functional electrocatalysts for water splitting and rechargeable zinc-air battery: A case of Pt nanoclusters on NiFe-LDH nanosheets. *Nano Energy* **2020**, *72*, 104669. [CrossRef]
46. Zhang, J.; Zhao, Y.; Guo, X.; Chen, C.; Dong, C.L.; Liu, R.S.; Han, C.P.; Li, Y. Gogotsi, Wang, G. Single platinum atoms immobilized on an MXene as an efficient catalyst for the hydrogen evolution reaction. *Nat. Catal.* **2018**, *1*, 985–992. [CrossRef]
47. Huang, K.; Wang, R.; Wu, H.; Wang, H.; He, X.; Wei, H.; Wang, S.; Zhang, R.; Lei, M.; Guo, W. Direct immobilization of an atomically dispersed Pt catalyst by suppressing heterogeneous nucleation at −40 °C. *J. Mater. Chem. A* **2019**, *7*, 25779–25784. [CrossRef]
48. Zhang, Z.; Chen, Y.; Zhou, L.; Chen, C.; Han, Z.; Zhang, B.; Wu, Q.; Yang, L.; Du, L.; Bu, Y.; et al. The simplest construction of single-site catalysts by the synergism of micropore trapping and nitrogen anchoring. *Nat. Commun.* **2019**, *10*, 1657. [CrossRef] [PubMed]
49. Li, B.; Ye, R.; Wang, Q.; Liu, X.; Fang, P.; Hu, J. Facile synthesis of coral-like Pt nanoparticles/MXene ($Ti_3C_2T_x$) with efficient hydrogen evolution reaction activity. *Ionics* **2021**, *27*, 1221–1231. [CrossRef]
50. Lim, K.R.G.; Handoko, A.D.; Johnson, L.R.; Meng, X.; Lin, M.; Subramanian, G.S.; Anasori, B.; Gogotsi, Y.; Vojvodic, A.; She, Z.W. 2H-MoS_2 on Mo_2CT_x MXene Nanohybrid for Efficient and Durable Electrocatalytic Hydrogen Evolution. *ACS Nano* **2020**, *14*, 16140–16155. [CrossRef]
51. Yan, L.; Zhang, B.; Wu, S.; Yu, J. A general approach to the synthesis of transition metal phosphide nanoarrays on MXene nanosheets for pH-universal hydrogen evolution and alkaline overall water splitting. *J. Mater. Chem. A* **2020**, *8*, 14234–14242. [CrossRef]
52. Liu, H.; Hu, Z.; Liu, Q.; Sun, P.; Wang, Y.; Chou, S.; Hu, Z.; Zhang, Z. Single-atom Ru anchored in nitrogen-doped MXene ($Ti_3C_2T_x$) as an efficient catalyst for the hydrogen evolution reaction at all pH values. *J. Mater. Chem. A* **2020**, *8*, 24710–24717. [CrossRef]
53. Peng, X.; Zhao, S.; Mi, Y.; Han, L.; Liu, X.; Qi, D.; Sun, J.; Liu, Y.; Bao, H.; Zhuo, L. Trifunctional Single-Atomic Ru Sites Enable Efficient Overall Water Splitting and Oxygen Reduction in Acidic Media. *Small* **2020**, *16*, 2002888. [CrossRef]
54. Wang, H.; Lin, Y.; Liu, S.; Li, J.; Bu, L.; Chen, J.; Xiao, X.; Choi, J.H.; Gao, L.; Lee, J.M. Confined growth of pyridinic N-Mo_2C sites on MXenes for hydrogen evolution. *J. Mater. Chem. A* **2020**, *8*, 7109–7116. [CrossRef]
55. Cheng, Y.; Dai, J.; Song, Y.; Zhang, Y. Single molybdenum atom anchored on 2D Ti_2NO_2 MXene as a promising electrocatalyst for N_2 fixation. *Nanoscale* **2019**, *11*, 18132–18141. [CrossRef] [PubMed]
56. Zhang, S.; Zhuo, H.; Li, S.; Bao, Z.; Deng, S.; Zhuang, G.; Zhong, X.; Wei, Z.; Yao, Z.; Wang, J.G. Effects of surface functionalization of MXene-based nanocatalysts on hydrogen evolution reaction performance. *Catal. Today* **2020**, *168*, 187–195. [CrossRef]
57. Wu, X.; Zhou, S.; Wang, Z.; Liu, J.; Pei, W.; Yang, P.; Zhao, J.; Qiu, J. Engineering multifunctional collaborative catalytic interface enabling efficient hydrogen evolution in all pH range and seawater. *Adv. Energy Mater.* **2019**, *9*, 1901333. [CrossRef]